Chemical Science

EDGE ARTICLE

View Article Online
View Journal | View Issue

Cite this: *Chem. Sci.*, 2019, **10**, 1410

All publication charges for this article have been paid for by the Royal Society of Chemistry

Received 23rd September 2018
Accepted 4th October 2018

DOI: 10.1039/c8sc04239j

rsc.li/chemical-science

Anion control of tautomeric equilibria: Fe–H *vs.* N–H influenced by NH···F hydrogen bonding†

Geoffrey M. Chambers, Samantha I. Johnson, Simone Raugei and R. Morris Bullock *

Counterions can play an active role in chemical reactivity, modulating reaction pathways, energetics and selectivity. We investigated the tautomeric equilibrium resulting from protonation of $Fe(P^{Et}N^{Me}P^{Et})(CO)_3$ ($P^{Et}N^{Me}P^{Et}$ = $(Et_2PCH_2)_2NMe$) at Fe or N. Protonation of $Fe(P^{Et}N^{Me}P^{Et})(CO)_3$ by $[(Et_2O)_2H]^+[B(C_6F_5)_4]^-$ occurs at the metal to give the iron hydride $[Fe(P^{Et}N^{Me}P^{Et})(CO)_3H]^+[B(C_6F_5)_4]^-$. In contrast, treatment with $HBF_4{\cdot}OEt_2$ gives protonation at the iron and at the pendant amine. Both the FeH and NH tautomers were characterized by single crystal X-ray diffraction. Addition of excess BF_4^- to the equilibrium mixture leads to the NH tautomer being exclusively observed, due to NH···F hydrogen bonding. A quantum chemical analysis of the bonding properties of these systems provided a quantification of hydrogen bonding of the NH to BF_4^- and to OTf^-. Treatment of $Fe(P^{Et}N^{Me}P^{Et})(CO)_3$ with excess HOTf gives a dicationic complex where both the iron and nitrogen are protonated. Isomerization of the dicationic complex was studied by NOESY NMR spectroscopy.

Introduction

Tautomerization has been extensively studied, the archetypal example being the keto–enol equilibrium of ketones and aldehydes.[1–3] Hydrogen bonding and other non-covalent interactions can profoundly influence tautomeric equilibria, and consequentially, affect the selectivity of catalytic reactions.[4] Tautomers play a key role in the structure and reactivity of transition metal complexes. Tautomeric equilibria between dihydrogen and dihydride complexes (eqn (1)) were identified early in the history of H_2 complexes.[5–11] Subsequent studies examined more deeply the properties of elongated dihydrogen complexes,[12,13] and the relationship between dihydrogen and dihydride tautomers.[14,15] Tautomeric equilibria between $M(\eta^2\text{-}SiH_4)$ complexes and $M(H)(SiH_3)$ complexes have also been observed.[16]

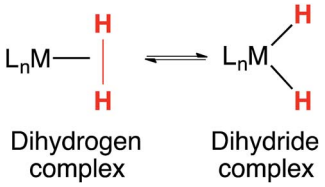

(1)

Proton transfers play a prominent role in catalysis. Studies on the kinetic and thermodynamic acidity of metal hydrides[17–19] and dihydrogen complexes[20] provide a foundation for understanding catalytic reactions that require proton transfers. Pendant amines in diphosphine ligands can function as proton relays,[21] leading to electrocatalysts for production of H_2 (ref. 22 and 23) and oxidation of H_2.[24,25] Studies of the intramolecular[26] and intermolecular[27] proton transfers in these systems has provided insight into the mechanisms of catalysis. Proton transfer between a pendant amine and a metal is often rapid, a feature that enhances catalytic rates. It has seldom been possible to separately observe or characterize the two tautomers.

Ion pairing can influence the thermodynamics and kinetics of transition metal chemistry, particularly those involving proton transfer reactions of metal hydrides.[28–31] Bifurcated hydrogen bonding of BF_4^- to two NH bonds was observed in a crystal structure of a di-iron complex.[32] Rauchfuss and co-workers found that excess BF_4^- shifted the equilibrium between Fe–H and N–H tautomers in a synthetic [FeFe]-hydrogenase model complex, increasing the amount of the ammonium tautomer.[33] The role of counterions on reactivity has been studied computationally,[34] with much of the work focusing on the influence of counterions on transition states and how they lower kinetic barriers[35] or change the regioselectivity in catalysis.[36,37] Poli, Shubina and co-workers reported computations showing how specific hydrogen bonding interactions between Mo dihydride complexes and BF_4^- could be altered by solvent choice, which ultimately determined the

Center for Molecular Electrocatalysis, Pacific Northwest National Laboratory, Richland, Washington 99352, USA. E-mail: morris.bullock@pnnl.gov

† Electronic supplementary information (ESI) available: Spectroscopic, electrochemical, crystallographic and computational details. CCDC 1810828 for $[\mathbf{1}]^+[BAr^F{}_4]^-$, 1810829 for $[\mathbf{FeNH}]^+BF_4^-$, 1810831 $\mathbf{Fe^0}$, 1810832 for $[\mathbf{FeH}]^+[B(C_6F_5)_4]^-$, 1849473 for $[\mathbf{FeHNH}]^{2+}[OTf^-]_2$, 1849476 for $[\mathbf{FeNH}]^+OTf^-$. For ESI and crystallographic data in CIF or other electronic format see DOI: 10.1039/c8sc04239j

thermodynamic equilibrium between Mo dihydrides and dihydrogen complexes.[30] Dub and Gordon suggested that hydrogen bonding between BF_4^- and H_2 ligands may influence enantioselective ketone hydrogenations.[38] Computations from Heinze and co-workers showed that non-covalent interactions between NO_2-substituted gold tetraarylporphyrins and PF_6^- counterion change the electronic structure from a metal-centered to a ligand-centered radical.[39]

Hydrogen bonding involving metal hydrides is especially interesting, as the M–H bond can engage in two different types of hydrogen bonding, as discussed in reviews by Shubina and co-workers[31,40–42] Crabtree[43] and Brammer.[44] Intramolecular Ir–H···H–N interactions were discovered independently and reported in 1994 by Morris[45] and by Crabtree.[46,47] In these examples, the M-H bond serves as the weak base (hydrogen bond acceptor). The protic–hydridic attraction ($H^{\delta+}\cdots H^{\delta-}$) in the "dihydrogen bond"[48] has been studied in many examples since these interactions were recognized. Intermolecular M–H···H–O interactions of metal hydrides have been characterized by extensive spectroscopic studies,[49] particularly in the interaction of metal hydrides with acidic alcohols. Studies of these dihydrogen bonds provide insights into details of hydrogen bonding preceding proton transfer reactions.[50–52] A Ru–H···H–N interaction is cleaved in reaction with CO_2, leading to a ruthenium formate complex.[53] In iron electrocatalysts for oxidation of H_2, an Fe–H···H–N dihydrogen bond was characterized by neutron diffraction, providing precise structural characterization.[54] NMR spectroscopy can provide evidence for dihydrogen bond formation; Manor and Rauchfuss found that the dihydrogen bond formed by addition of $HNMe_3^+$ to a hydride bridging Fe and Ni led to a change of about 2 ppm in the ^{1}H NMR chemical shift.[55]

Metal hydrides exhibit versatile reactivity patterns; in addition to the hydrogen bonds described above, metal hydrides engage in hydrogen bonding where the M–H bond is the weak acid, or hydrogen bond donor. Early examples were reported for hydrogen bonding between cationic metal hydrides and the P=O bonds of phosphine oxides, such as $Ph_3P{=}O$.[56,57] Subsequent detailed studies showed that neutral metal hydrides engage in intermolecular hydrogen bonding with phosphine oxides or amines.[58] Hydrogen bonding has been found between dihydrogen ligands and BF_4^- (ref. 59) or OTf^- anions.[60]

We report here that protonation of $Fe(P^{Et}N^{Me}P^{Et})(CO)_3$ ($P^{Et}N^{Me}P^{Et} = (Et_2PCH_2)_2NMe$) can occur at either the N, or the Fe, or both. Singly protonated N–H and Fe–H tautomers were isolated, and their structures were characterized by X-ray diffraction. The preference for protonation at N or Fe is strongly influenced by the counterion; addition of BF_4^- to Fe–H tautomer converts it to the N–H tautomer. Computational studies provide insights into the N–H···F hydrogen bonding that strongly influences the tautomeric equilibria. The doubly protonated complex resulting from protonation at both N and Fe has been characterized by spectroscopic and crystallographic studies, and is shown to exist as an interconverting mixture of isomers.

Results and discussion

Synthesis and characterization of Fe(diphosphine)$(CO)_3$ complexes

The iron complex $Fe(P^{Et}N^{Me}P^{Et})(CO)_3$ (**Fe^0**) is prepared by heating toluene solutions of $Fe(COT)(CO)_3$ (COT = cyclooctatetraene) and $P^{Et}N^{Me}P^{Et}$ to 110 °C (eqn (2)). It is purified by chromatography and isolated in 78% yield as a pale yellow, mildly air-sensitive microcrystalline crystalline solid. The aniline derivative $Fe(P^{Et}N^{Ph}P^{Et})(CO)_3$ ($P^{Et}N^{Ph}P^{Et} = (Et_2PCH_2)_2$-NPh) was prepared in a similar manner. The solid state structure of **Fe^0** was determined by single crystal X-ray diffraction (Fig. 1). The iron adopts a trigonal bipyramidal geometry with the diphosphine spanning an axial and equatorial site.

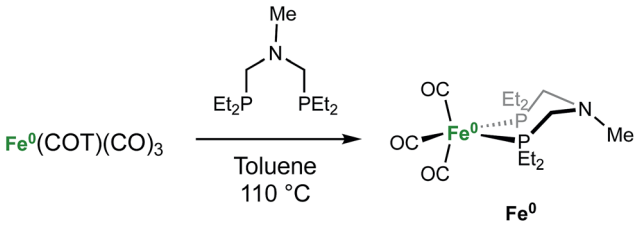

(2)

Only one phosphorus resonance is observed in the $^{31}P\{^1H\}$ NMR spectra of **Fe^0** at room temperature, indicating that the structures are fluxional in solution. The ^{1}H NMR spectrum of **Fe^0** shows a single resonance for the N–Me protons and the PCH_2N methylene groups, consistent with rapid inversion of the nitrogen center. The IR spectrum of **Fe^0** in CH_2Cl_2 solution has three bands ($\tilde{\nu}_{CO}$ = 1976, 1900, 1873 cm^{-1}).

Protonation and tautomerization studies

Protonation of **Fe^0** with $[(Et_2O)_2H]^+[B(C_6F_5)_4]^-$ occurs at the metal to give a cationic iron hydride complex (Scheme 1). After crystallization from Et_2O/*n*-pentane, the hydrides $[Fe(P^{Et}N^{Me}P^{Et})(CO)_3H]^+[B(C_6F_5)_4]^-$ (**[FeH]$^+$**$[B(C_6F_5)_4]^-$) and $[Fe(P^{Et}N^{Ph}P^{Et})(CO)_3H]^+[B(C_6F_5)_4]^-$ were isolated as white solids. The structure of **[FeH]$^+$**$[B(C_6F_5)_4]^-$ was determined by X-ray

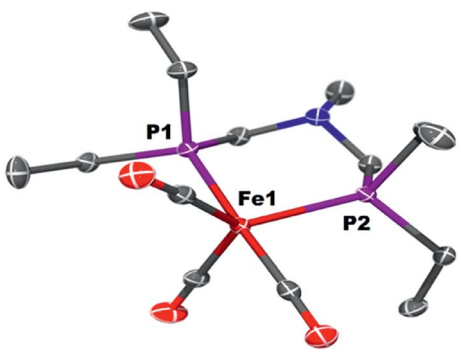

Fig. 1 Solid state structure of $Fe(P^{Et}N^{Me}P^{Et})(CO)_3$ (**Fe^0**). Thermal ellipsoids shown at the 50% probability level. Hydrogen atoms are omitted.

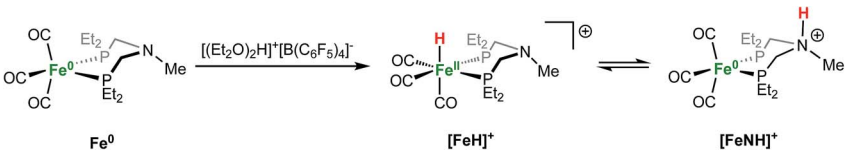

Scheme 1

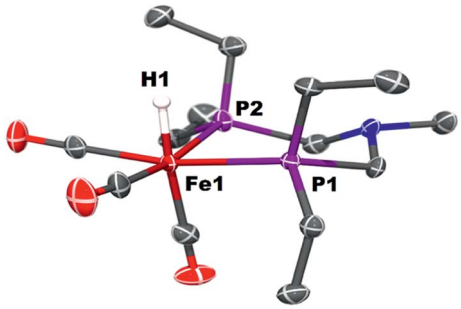

Fig. 2 Solid state structure of $[Fe(P^{Et}N^{Me}P^{Et})(CO)_3H]^+[B(C_6F_5)_4]^-$, **[FeH]$^+$**. Thermal ellipsoids shown at the 50% probability level. All other hydrogen atoms except the Fe–H are omitted.

crystallography (Fig. 2). The metal hydride resonance of **[FeH]$^+$** is observed in the ^{1}H NMR spectrum as a triplet at δ −9.27 (t, $^2J_{PH}$ = 45 Hz). Treatment of solutions of the iron hydrides with NEt_3 gives the corresponding neutral Fe(0) compounds, demonstrating reversible protonation.

Protonation of **Fe^0** with $HBF_4{\cdot}OEt_2$ in CH_2Cl_2 gives protonation at both the Fe and the pendant amine. Monitoring the reaction by IR spectroscopy (Fig. 3) shows $\tilde{\nu}_{CO}$ bands at 1992, 1920, and 1894 cm^{-1} assigned to the amine-protonated isomer **[FeNH]$^+$**, along with bands for **[FeH]$^+$**. The shift in the $\tilde{\nu}_{CO}$ bands to higher energy in **[FeNH]$^+$** relative to **Fe^0** is consistent with the overall positive charge of **[FeNH]$^+$**, and the relatively lower energy of the $\tilde{\nu}_{CO}$ bands compared to **[FeH]$^+$** is consistent with the difference in formal oxidation state between the two tautomers.

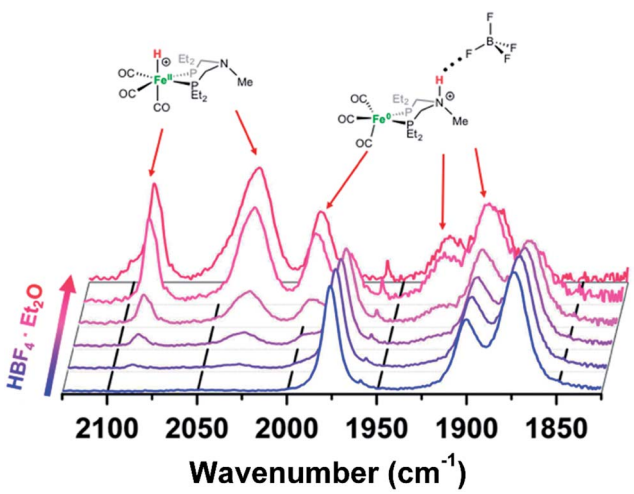

Fig. 3 IR spectra ($\tilde{\nu}_{CO}$ region) of **Fe^0** treated with varying amounts of $HBF_4{\cdot}OEt_2$ in CH_2Cl_2. Blue = **Fe^0** in CH_2Cl_2 solution before addition of acid. Red = spectrum after 1 equiv. of $HBF_4{\cdot}OEt_2$.

Crystals of the protonated amine tautomer, **[FeNH]$^+$**BF_4^-, were obtained from the reaction mixture from MeCN/Et_2O solutions, and its structure was determined by X-ray crystallography (Fig. 4). The NH···F distance was found to be 1.93(1) Å, consistent with the presence of NH···F hydrogen bonding of the protonated amine to an F of the BF_4^- anion. Structural studies of organic compounds with protonated amines with BF_4^- counterions show NH···F hydrogen bonding.[61,62] Infrared spectroscopy (KBr) of the crystallized **[FeNH]$^+$**BF_4^- gave $\tilde{\nu}_{CO}$ bands similar to those assigned to **[FeNH]$^+$** in the solution spectra shown in Fig. 3. The triflate derivate was also prepared by protonation of **Fe^0** with HOTf, and **[FeNH]$^+$**OTf^- was also characterized crystallographically (Fig. 5).

To determine the influence of the anion BF_4^- on the equilibrium between **[FeH]$^+$** and **[FeNH]$^+$**, solutions of **[FeH]$^+$**$[B(C_6F_5)_4]^-$ were treated with $[Et_4N]^+BF_4^-$. Treatment of CH_2Cl_2 solutions of **[FeH]$^+$**$[B(C_6F_5)_4]^-$ with less than 1 equiv. of $[Et_4N]^+BF_4^-$ gives IR spectra indicating a preference for **[FeH]$^+$**. As more $[Et_4N]^+BF_4^-$ is added, **[FeNH]$^+$** becomes the preferred tautomer. At high concentrations of $[Et_4N]^+BF_4^-$, the Fe–H isomer is no longer detected (Fig. 6). These results suggest that hydrogen bonding of N–H to BF_4^- dramatically influences the equilibrium because of the formation of an NH···F hydrogen bond. When monitored by ^{1}H spectroscopy, isolated single crystals of **[FeNH]$^+$**BF_4^- in CD_2Cl_2/THF-d_8 (95 : 5) solution treated with $K^+[B(C_6F_5)_4]^-$ give **[FeH]$^+$**, as determined by ^{1}H NMR spectroscopy, concomitant with precipitation of KBF_4 (Fig. S11†). Similarly, the hydride resonance in CD_2Cl_2 solutions of **[FeH]$^+$**$[B(C_6F_5)_4]^-$ is no longer observed following treatment with $[Et_4N]^+BF_4^-$ (Fig. S12†).

Recognizing the precedents cited above for hydrogen bonding involving metal hydrides, we considered whether

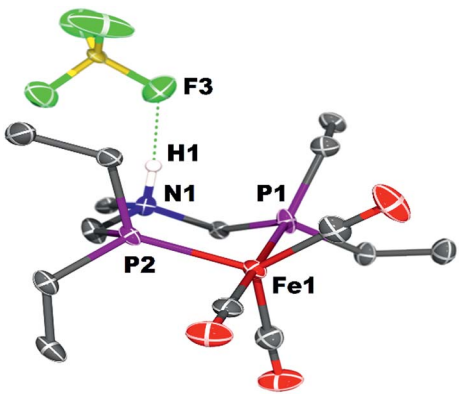

Fig. 4 Solid state structure of **[FeNH]$^+$**BF_4^-. Thermal ellipsoids shown at the 50% probability level. Hydrogen atoms other than the NH are omitted.

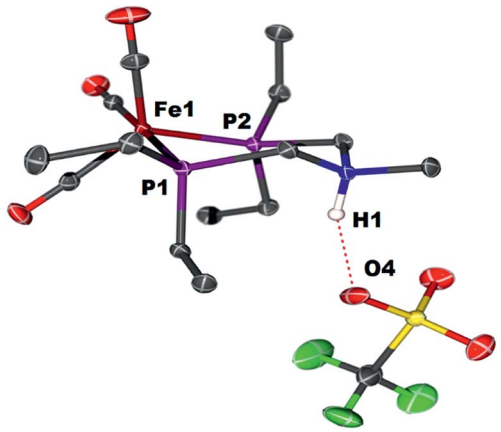

Fig. 5 Solid state structure of **[FeNH]**$^{+}$OTf^{-}. Thermal ellipsoids shown at the 50% probability level. All hydrogen atoms have been omitted except for the ammonium hydrogen.

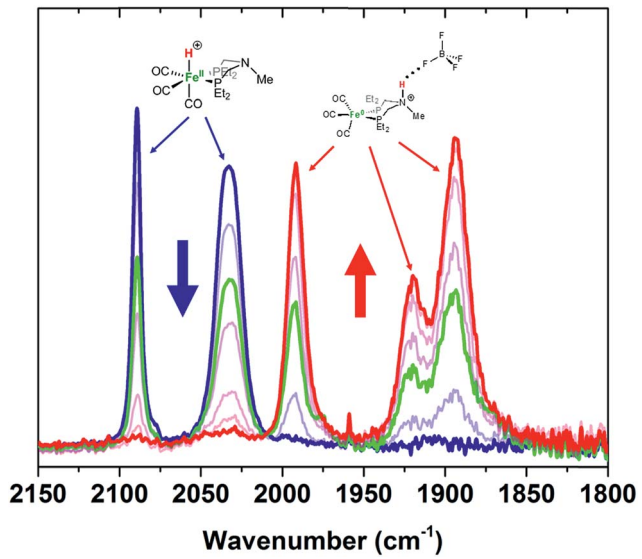

Fig. 6 IR spectra of a solution (≈10 mM) of **[FeH]**$^{+}$[B(C$_6$F$_5$)$_4$]$^{-}$ in CH_2Cl_2 treated with increasing amounts of [Et$_4$N]$^{+}$BF$_4^{-}$. Blue = **[FeH]**$^{+}$[B(C$_6$F$_5$)$_4$]$^{-}$. Green = **[FeH]**$^{+}$[B(C$_6$F$_5$)$_4$]$^{-}$ with ~1 equiv. of [Et$_4$N]$^{+}$BF$_4^{-}$. Red = **[FeH]**$^{+}$[B(C$_6$F$_5$)$_4$]$^{-}$ with ~5 equiv. of [Et$_4$N]$^{+}$BF$_4^{-}$.

hydrogen bonding of the Fe–H bond of **[FeH]**$^{+}$ to BF$_4^{-}$ might provide some stabilization. As a more direct probe of that possible interaction, we examined a related complex that does not have a pendant amine in the diphosphine ligand. Addition of 94 mM [Et$_4$N]$^{+}$BF$_4^{-}$ to a CD_2Cl_2 solution of [FeH(depp)(CO)$_3$]$^{+}$[B(C$_6$F$_5$)$_4$]$^{-}$ (depp = 1,3-bis(diethylphosphino)propane) led to a shift of the ^{1}H NMR resonance of the hydride from δ −9.028 (triplet, J_{PH} = 44.8 Hz) to δ −9.045. A further shift to δ −9.066 was observed following addition of 280 mM [Et$_4$N]$^{+}$BF$_4^{-}$ to the solution. We interpret these relatively small ^{1}H NMR spectroscopic shifts to indicate weak, if any, hydrogen bonding of the Fe–H to the BF$_4^{-}$ anion.

A search of the Cambridge Structural Database was carried out for cationic Fe hydrides with two or more Fe–P bonds and a BF$_4^{-}$ counterion. The structure[63] of {FeH[P(CH$_2$CH$_2$PPh$_2$)$_3$]}$^{+}$ BF$_4^{-}$ reveals a Fe–H···F separation of 2.91 Å, and an Fe–H···F separation of 3.40 Å was found[64] in [FeH(CO)$_3$(dppf)]$^{+}$BF$_4^{-}$ (dppf = 1,1′-bis(diphenylphosphino)ferrocene). The location of the hydride ligand is usually subject to uncertainty when determined by X-ray diffraction, so that will potentially make these comparisons less precise. Compared to the sum of the van der Waals radii of H and F (about 2.67 Å), these structures indicate that any Fe–H···F interactions are, at most, weak. The shortest H···F distance in the cationic molybdenum hydride, [Cp*MoH(PMe$_3$)$_3$]$^{+}$PF$_6^{-}$, is 3.33 Å.[65] While that distance is longer than would normally be considered a hydrogen bond, a computational study provided evidence for a weak interaction.

Computational studies of the influence of the anion

Structures of **[FeH]**$^{+}$, **[FeNH]**$^{+}$, **[FeNH]**$^{+}$BF$_4^{-}$, and **[FeNH]**$^{+}$OTf^{-} were optimized computationally, and the bonding properties were analyzed in the natural bond orbital (NBO)[66] theory framework, as discussed below. Both anions have a similar overall effect on the structure of **[FeNH]**$^{+}$. Without any anion, the N–H bond of **[FeNH]**$^{+}$ tucks in towards the Fe, with an Fe···H distance of 2.51 Å (Fig. S32†). When the counterion is added, the N–H bond moves away from the Fe. For comparison, the Fe···H distance is 3.59 Å in **[FeNH]**$^{+}$BF$_4^{-}$ and 3.69 Å in **[FeNH]**$^{+}$OTf^{-}. The computed N···F distance of 2.60 Å in **[FeNH]**$^{+}$BF$_4^{-}$ is nearly identical to the computed N···O distance of 2.59 Å in **[FeNH]**$^{+}$OTf^{-} (Fig. 7). However, the N–H bond length in **[FeNH]**$^{+}$BF$_4^{-}$ (1.07 Å) is shorter than in **[FeNH]**$^{+}$OTf^{-} (1.10 Å), suggesting a stronger N–H···X interaction in the latter.

Our calculations clearly show that anions can provide energetic stabilization of the N-protonated ligand. The calculated **[FeH]**$^{+}$ → **[FeNH]**$^{+}$ isomerization free energy of ΔG^0 = −2.5 kcal mol^{-1} shifts to −2.0 kcal mol^{-1} and −8.2 kcal mol^{-1}, when BF$_4^{-}$ or OTf^{-} are added. The nearly isoergic formation of **[FeNH]**$^{+}$BF$_4^{-}$ is consistent with the experimental observation of both tautomers being present at a 1 : 1 ratio of the iron complex to BF$_4^{-}$.

The strength of hydrogen bonds between the anion and the protonated amine was calculated in the NBO framework.[66] From an electronic standpoint, the formation of a hydrogen bond is accompanied by a sizeable charge transfer from the lone pair n(X) of the hydrogen bond acceptor to the σ*(N–H) anti-bonding orbital of the donor. The energy stabilization due to the hydrogen bond between **[FeNH]**$^{+}$ and the counterion is given by the ratio of the off-diagonal components of the Fock matrix and the difference in energy between the two orbitals.[66] This analysis also gives an estimate of the amount of charge transferred, q_{CT}, from the donor orbital to the acceptor orbital using eqn (3), wherein $\Delta E^{(2)}_{n\sigma^*}$ is the energy lowering, and the denominator represents the difference in orbital energies.[66]

$$q_{CT} \cong \frac{\left|\Delta E^{(2)}_{n\sigma^*}\right|}{\varepsilon_{\sigma^*} - \varepsilon_n} \quad (3)$$

For comparison, the interaction between N–H and one Cl of dichloromethane solvent was calculated. The calculated

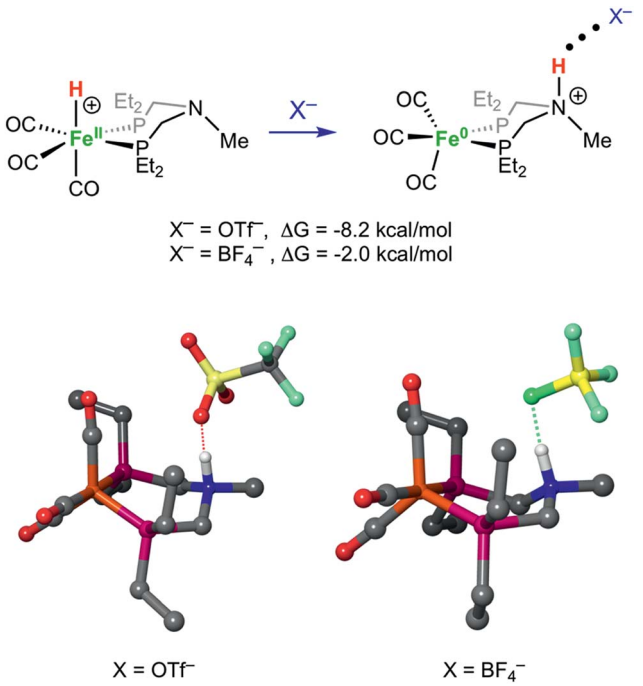

Fig. 7 The tautomer with a protonated amine ligand is favored with a OTf^- or BF_4^- counterion, as shown by DFT calculations. The computed structures of $[FeNH]^+OTf^-$ and $[FeNH]^+BF_4^-$ are shown in the lower part of the figure. Hydrogen atoms have been omitted, except for the protonated ammonium.

Table 1 Computed charge transfer and stabilization energies in $[FeNH]^+$

Interaction	Total charge transfer, q_{CT}	Stabilization energy, $\Delta E^{(2)}_{n\sigma^*}$ (kcal mol^{-1})
N–H···$ClCH_2Cl$	0.0004	0.2
N–H···FBF_3	0.0220	14.8
N–H···OTf	0.0399	20.3

$\Delta E^{(2)}_{n\sigma^*}$ and q_{CT} values are reported in Table 1. The magnitude of the charge transfer from both anions is comparable to values calculated for hydrogen bonding interactions between anions and water.[67] The second-order stabilization energy between the complex and BF_4^- and OTf^- is $\Delta E^{(2)}_{n\sigma^*}$ = 14.8 and 20.3 kcal mol^{-1}, respectively. The charge transfer and stabilization energy from both anions is orders of magnitude larger than the negligible stabilization energy from dichloromethane solvent. This result implies that the hydrogen bonding interaction is significant, and not merely the result of an interaction between an electronegative atom and the N–H bond. Further details of the contributing interactions are provided in the ESI.†

In contrast to the results with the protonated pendant amine, there is no donation from the lone pair of F to the Fe–H. This is not surprising, in view of the hydridic nature of the Fe–H, compared to the protic nature of the N–H. The atomic charge of the H of the ammonium was calculated to be +0.46, which contrasts greatly with the calculated value of −0.05 when bound to iron. Thus, the interaction between the hydride and the counterion will be repulsive, which is indicated by the energetics (ΔG = 7.9 kcal mol^{-1}) shown in Fig. S33.† Indeed, the small stabilization due to the interaction between the iron hydride bonding orbital, σ(Fe–H), and the four B–F antibonding orbitals, σ*(B–F), does not compensate for the overall electrostatic repulsion. The delocalized nature of the σ(Fe–H)-to-σ*(B–F) interaction is indicated by the geometry, wherein the BF_4^- anion is close to the hydride, with three fluorine atoms oriented toward the hydride, rather than the directed interaction seen in the geometry of the protonated amine complex. It is important to note that the σ(Fe–H)-to-σ*(B–F) interaction is much smaller than the σ(N–H)-to-σ*(B–F) interaction. Summing all of the stabilization energies gives $\Delta E^{(2)}_{\sigma\sigma^*}$ = 3.0 kcal mol^{-1}, for the Fe–H BF_4^- interaction, which is far less than the $\Delta E^{(2)}_{\sigma\sigma^*}$ = 15 kcal mol^{-1} exhibited by the interaction with between the N–H and BF_4^-.

Protonation at both Fe and N to give a dication

When **Fe^0** is treated with excess $HBF_4{\cdot}OEt_2$ or HOTf, protonation at both Fe and N is observed, giving a dication (Scheme 2). The doubly protonated complex, $[FeHNH]^{2+}[OTf^-]_2$, was characterized crystallographically (Fig. 8), showing one OTf^- that is hydrogen bonded to the N–H, and one OTf^- counterion that is not interacting. This dicationic complex exhibits a notably shorter NH···O distance (1.80(3) Å) relative to the monoprotonated complex $[FeNH]^+OTf^-$ (1.89(3) Å), suggesting a stronger hydrogen bonding interaction. The IR spectra of the doubly protonated $[FeHNH]^{2+}[BF_4^-]_2$ and $[FeHNH]^{2+}[OTf^-]_2$ complexes feature $\tilde{\nu}_{CO}$ bands shifted to higher energy relative to $[FeH]^+$; the difference is similar to that observed between **Fe^0** and $[FeNH]^+$.

^{1}H NMR spectra in CD_3CN solution of crystals of $[FeHNH]^{2+}[OTf^-]_2$ reveal multiple isomers. At 25 °C, two distinct species are indicated by two ammonium NH resonances (δ 9.40 and 8.89) and two hydride resonances (δ −9.62 and −9.71). These isomers are assigned to the *syn* (chair) and *anti* isomers, differing in the relative orientation of the FeH and NH (Scheme 3). The NOESY spectrum of $[FeHNH]^{2+}[OTf^-]_2$ at 25 °C (Fig. S17†) shows an exchange correlation between the FeH and

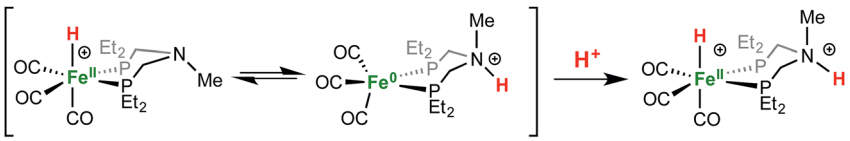

Scheme 2

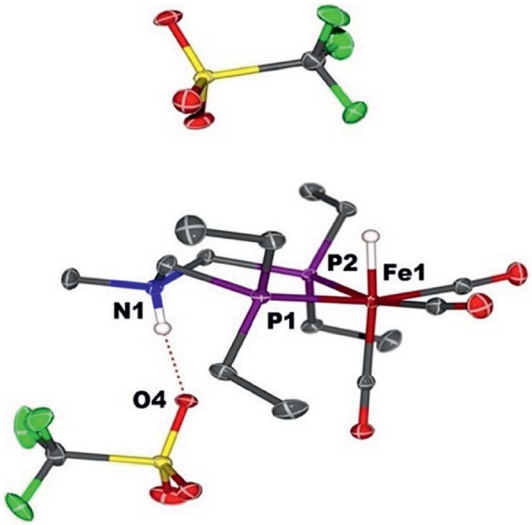

Fig. 8 Solid state structure of $[FeHNH]^{2+}[OTf^{-}]_2$. Thermal ellipsoids are shown at the 50% probability level. Hydrogen atoms are omitted, except the N–H and Fe–H.

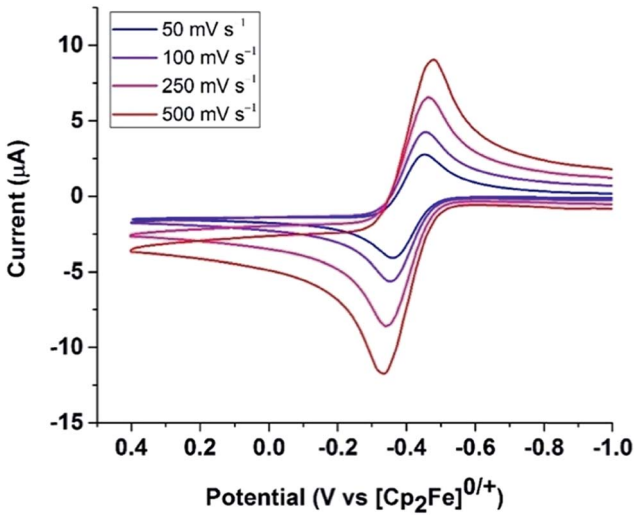

Fig. 9 Cyclic voltammogram of Fe^0 in PhF under Ar at various scan rates, showing a reversible oxidation at $E_{1/2} = -0.37$ V *vs.* $[Cp_2Fe]^{0/+}$. Conditions: $[Bu_4N][B(C_6F_5)_4]$ (100 mM) as the supporting electrolyte, glassy carbon as the working electrode, a silver wire as a pseudo reference, and a Pt wire as the counter electrode.

NH resonance of one isomer, proposed to be the *syn* isomer. An additional exchange correlation is observed between the NH resonances of the two isomers, consistent with interconversion between *syn* (chair) and *anti* isomers.

At −40 °C, a broad resonance observed at δ 7.11 is proposed to arise from a third isomer in which the FeH and NH are *syn* and the six-membered ligand ring adopts a boat conformation, bringing the FeH and NH in close proximity. The FeH and NH in the *syn* (boat) isomer are likely stabilized to some extent by dihydrogen bonding[48] between the hydridic $FeH^{\delta-}$ and the protic $NH^{\delta+}$.[54] Computational analysis shows $\Delta E^{(2)}_{\sigma\sigma^*} = 2.9$ kcal mol^{-1} in the presence of counterion. A more detailed discussion of this dihydrogen bonding is provided in the ESI.† The NOESY spectrum at −40 °C (Fig. S18†) shows an exchange correlation of the FeH only with the NH resonance of the *syn* (boat) isomer, presumably occurring through an unobserved $Fe(H_2)^+$ intermediate.[54,68]

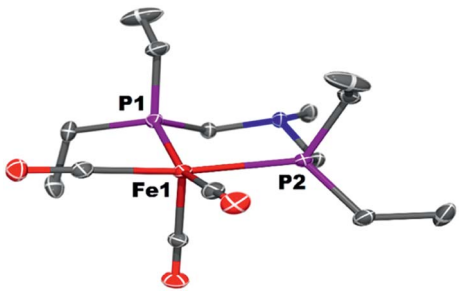

Fig. 10 Solid state structure of $[Fe^{I}]^+[BAr^F{}_4]^-$. Thermal ellipsoids are shown at the 15% probability level. X-ray diffraction data were collected at 230 K because of fracture of the crystal at lower temperatures. Two molecules were present in the asymmetric unit; both are similar, and one molecule was chosen arbitrarily to be represented here.

Preparation, isolation and reactions of stable 17e$^-$ Fe cations

The cyclic voltammogram of $\mathbf{Fe^0}$ (Fig. 9) in fluorobenzene shows a reversible one-electron oxidation at −0.37 V *vs.* $Cp_2Fe^{0/+}$.

Oxidation of $\mathbf{Fe^0}$ by $[Cp_2Fe]^+[BAr^F{}_4]^-$ (1 equiv.; Ar^F = 3,5-bis(trifluoromethyl)phenyl) resulted in an immediate color change of the solution from yellow to dark green. The paramagnetic complex $[Fe(P^{Et}N^{Me}P^{Et})(CO)_3]^+[BAr^F{}_4]^-$, $\mathbf{[Fe^I]^+}$, was isolated as air-sensitive dark green crystals. X-Band EPR spectroscopy of $\mathbf{[Fe^I]^+}$ at 22 °C gives $g_{iso} = 2.05$ and a phosphorus hyperfine coupling $A_{iso} = 63$ MHz (see ESI†), similar to spectra reported for related complexes.[64,69] The 17-electron iron center adopts a square pyramidal geometry, as indicated by X-ray crystallography (Fig. 10). The carbonyl stretching frequencies ($\tilde{\nu}_{CO}$ = 2069, 2007, 1999 cm^{-1}) shift to higher energies compared to **1**, consistent with reduced backbonding in the cationic iron complex.

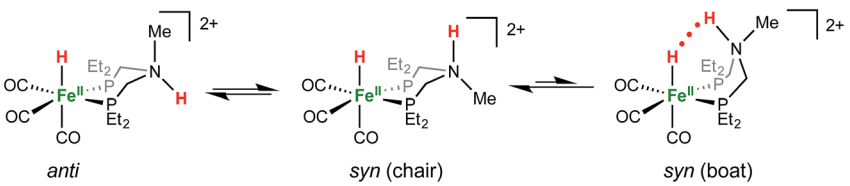

Scheme 3

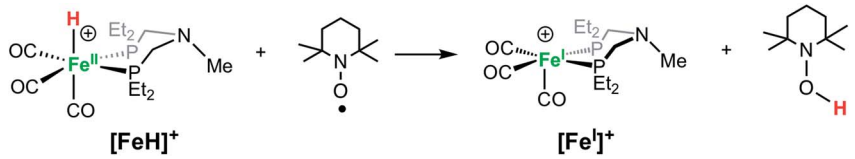

(4)

Solutions of $[\mathbf{FeH}]^+BF_4^-$ treated with TEMPO (2,2,6,6-tetramethylpiperidin-1-oxyl) immediately become dark green, converting the hydride to $[\mathbf{Fe^I}]^+$, as confirmed by IR spectroscopy (eqn (4)). Rauchfuss and co-workers reported similar reaction proceeding through a proton-coupled electron transfer reaction in studies of [FeFe]-hydrogenase model complexes with pendant amines, in which the protonated amine form is strongly favored.[70]

Reactions of Fe^I complexes with H_2 are seldom reported, but Peters and co-workers reported a Fe^I complex that reacts with H_2 to generate a rare $Fe^I(H_2)$ complex.[71] We found that dark green solutions of $[\mathbf{Fe^I}]^+$ react slowly with H_2 (1 atm) to give pale yellow solutions of the hydride $[\mathbf{FeH}]^+$, but the reaction is slow, occurring over a few days. When monitored by ^1H NMR spectroscopy, the broad resonances of the paramagnetic complex $[\mathbf{Fe^I}]^+$ decrease, and new resonances appear, corresponding to the iron hydride $[\mathbf{FeH}]^+$, but unidentified side products are observed. The yield of $[\mathbf{FeH}]^+$ was determined to be approximately 60% by integration against an internal standard. Camara and Rauchfuss reported[72] that the reaction of a [FeFe]-hydrogenase complex with H_2 is accelerated by a one-electron oxidation, even though that oxidant is not capable of oxidizing the complex. We carried out the reaction of $[\mathbf{Fe^I}]^+$ with H_2 with added $[Cp_2Fe]^+$, but the reaction rate and yield were similar to that observed with no oxidant added. The very slow reaction with H_2 and the low yield of the iron hydride preclude using $[\mathbf{Fe^I}]^+$ as a competent electrocatalyst for H_2 oxidation.

Conclusion

Protonation of the iron diphosphine complex $Fe(P^{Et}N^{Me}P^{Et})(CO)_3$ occurs at Fe and the amine, generating tautomers. The iron hydride complex $[Fe(P^{Et}N^{Me}P^{Et})(CO)_3H]^+[B(C_6F_5)_4]^-$ is converted to the N–H tautomer, with a protonated amine, by addition of excess $[Et_4N]^+BF_4^-$. Both isomers were characterized by spectroscopy and X-ray crystallography. Control of the tautomeric equilibrium occurs because of the favorable formation of an NH···F hydrogen bonding interaction between the protonated amine and the BF_4^- anion. Quantum chemical calculations quantified the strength of hydrogen bonding and its influence on the equilibrium. Protonation of $Fe(P^{Et}N^{Me}P^{Et})(CO)_3$ with an excess of HOTf gives a doubly protonated dication with Fe–H and N–H bonds. The dication exists as interconverting isomers in solution, as determined by 2D NMR spectroscopic studies.

Conflicts of interest

There are no conflicts to declare.

Acknowledgements

This work was supported as part of the Center for Molecular Electrocatalysis, an Energy Frontier Research Center funded by the U.S. Department of Energy, Office of Science, Office of Basic Energy Sciences. Pacific Northwest National Laboratory (PNNL) is operated by Battelle for the U.S. DOE. We thank Dr Eric Walter for the EPR spectra. EPR experiments were performed using the Environmental Molecular Sciences Laboratory (EMSL), a National Scientific User Facility sponsored by the DOE's Office of Biological and Environmental Research and located at PNNL. Computations were performed using the Cascade supercomputer at EMSL.

References

1 Y. Chiang, A. J. Kresge, Y. S. Tang and J. Wirz, *J. Am. Chem. Soc.*, 1984, **106**, 460–462.
2 A. J. Kresge, *Acc. Chem. Res.*, 1990, **23**, 43–48.
3 Z. Rappoport and S. E. Biali, *Acc. Chem. Res.*, 1988, **21**, 442–449.
4 H. J. Davis and R. J. Phipps, *Chem. Sci.*, 2017, **8**, 864–877.
5 G. J. Kubas, R. R. Ryan and D. A. Wrobleski, *J. Am. Chem. Soc.*, 1986, **108**, 1339–1341.
6 G. J. Kubas, C. J. Unkefer, B. I. Swanson and E. Fukushima, *J. Am. Chem. Soc.*, 1986, **108**, 7000–7009.
7 M. S. Chinn and D. M. Heinekey, *J. Am. Chem. Soc.*, 1987, **109**, 5865–5867.
8 M. S. Chinn and D. M. Heinekey, *J. Am. Chem. Soc.*, 1990, **112**, 5166–5175.
9 X.-L. Luo and R. H. Crabtree, *J. Am. Chem. Soc.*, 1990, **112**, 6912–6918.
10 K. A. Earl, G. Jia, P. A. Maltby and R. H. Morris, *J. Am. Chem. Soc.*, 1991, **113**, 3027–3039.
11 G. J. Kubas, *Chem. Rev.*, 2007, **107**, 4152–4205.
12 J. K. Law, H. Mellows and D. M. Heinekey, *J. Am. Chem. Soc.*, 2001, **123**, 2085–2086.
13 J. K. Law, H. Mellows and D. M. Heinekey, *J. Am. Chem. Soc.*, 2002, **124**, 1024–1030.
14 D. M. Heinekey, A. Lledos and J. M. Lluch, *Chem. Soc. Rev.*, 2004, **33**, 175–182.
15 R. H. Morris, *Coord. Chem. Rev.*, 2008, **252**, 2381–2394.

16 X.-L. Luo, G. J. Kubas, C. J. Burns, J. C. Bryan and C. J. Unkefer, *J. Am. Chem. Soc.*, 1995, **117**, 1159–1160.
17 E. J. Moore, J. M. Sullivan and J. R. Norton, *J. Am. Chem. Soc.*, 1986, **108**, 2257–2263.
18 R. T. Edidin, J. M. Sullivan and J. R. Norton, *J. Am. Chem. Soc.*, 1987, **109**, 3945–3953.
19 S. S. Kristjánsdóttir and J. R. Norton, in *Transition Metal Hydrides*, ed. A. Dedieu, VCH, New York, 1991, ch. 9, pp. 309–359.
20 R. H. Morris, *Chem. Rev.*, 2016, **116**, 8588–8654.
21 D. L. DuBois, *Inorg. Chem.*, 2014, **53**, 3935–3960.
22 A. J. P. Cardenas, B. Ginovska, N. Kumar, J. Hou, S. Raugei, M. L. Helm, A. M. Appel, R. M. Bullock and M. O'Hagan, *Angew. Chem., Int. Ed.*, 2016, **55**, 13509–13513.
23 S. Raugei, M. L. Helm, S. Hammes-Schiffer, A. M. Appel, M. O'Hagan, E. S. Wiedner and R. M. Bullock, *Inorg. Chem.*, 2016, **55**, 445–460.
24 T. Liu, D. L. DuBois and R. M. Bullock, *Nat. Chem.*, 2013, **5**, 228–233.
25 R. M. Bullock and M. L. Helm, *Acc. Chem. Res.*, 2015, **48**, 2017–2026.
26 M. O'Hagan, W. J. Shaw, S. Raugei, S. Chen, J. Y. Yang, U. J. Kilgore, D. L. DuBois and R. M. Bullock, *J. Am. Chem. Soc.*, 2011, **133**, 14301–14312.
27 M. O'Hagan, M. H. Ho, J. Y. Yang, A. M. Appel, M. Rakowski DuBois, S. Raugei, W. J. Shaw, D. L. DuBois and R. M. Bullock, *J. Am. Chem. Soc.*, 2012, **134**, 19409–19424.
28 A. Macchioni, *Chem. Rev.*, 2005, **105**, 2039–2074.
29 M. G. Basallote, M. Besora, C. E. Castillo, M. J. Fernandez-Trujillo, A. Lledos, F. Maseras and M. A. Manez, *J. Am. Chem. Soc.*, 2007, **129**, 6608–6618.
30 P. A. Dub, N. V. Belkova, O. A. Filippov, J.-C. Daran, L. M. Epstein, A. Lledós, E. S. Shubina and R. Poli, *Chem.–Eur. J.*, 2010, **16**, 189–201.
31 N. V. Belkova, L. M. Epstein, O. A. Filippov and E. S. Shubina, *Chem. Rev.*, 2016, **116**, 8545–8587.
32 P. Das, J.-F. Capon, F. Gloaguen, F. Y. Petillon, P. Schollhammer and J. Talarmin, *Inorg. Chem.*, 2004, **43**, 8203–8205.
33 M. E. Carroll, B. E. Barton, T. B. Rauchfuss and P. J. Carroll, *J. Am. Chem. Soc.*, 2012, **134**, 18843–18852.
34 G. Jindal, H. K. Kisan and R. B. Sunoj, *ACS Catal.*, 2015, **5**, 480–503.
35 M. C. Groenenboom and J. A. Keith, *J. Phys. Chem. B*, 2016, **120**, 10797–10807.
36 M. Arthuis, R. Beaud, V. Gandon and E. Roulland, *Angew. Chem., Int. Ed.*, 2012, **51**, 10510–10514.
37 V. M. Lau, W. C. Pfalzgraff, T. E. Markland and M. W. Kanan, *J. Am. Chem. Soc.*, 2017, **139**, 4035–4041.
38 P. A. Dub and J. C. Gordon, *Dalton Trans.*, 2016, **45**, 6756–6781.
39 S. Preiß, J. Melomedov, A. Wünsche von Leupoldt and K. Heinze, *Chem. Sci.*, 2016, **7**, 596–610.
40 N. V. Belkova, L. M. Epstein and E. S. Shubina, *Eur. J. Inorg. Chem.*, 2010, **2010**, 3555–3565.
41 N. V. Belkova, E. S. Shubina and L. M. Epstein, *Acc. Chem. Res.*, 2005, **38**, 624–631.
42 L. M. Epstein and E. S. Shubina, *Coord. Chem. Rev.*, 2002, **231**, 165–181.
43 R. H. Crabtree, *J. Organomet. Chem.*, 1998, **577**, 111–115.
44 L. Brammer, *Dalton Trans.*, 2003, 3145–3157.
45 A. J. Lough, S. Park, R. Ramachandran and R. H. Morris, *J. Am. Chem. Soc.*, 1994, **116**, 8356–8357.
46 E. Peris, J. C. Lee Jr and R. H. Crabtree, *J. Chem. Soc., Chem. Commun.*, 1994, 2573.
47 J. C. Lee Jr, E. Peris, A. L. Rheingold and R. H. Crabtree, *J. Am. Chem. Soc.*, 1994, **116**, 11014–11019.
48 R. Custelcean and J. E. Jackson, *Chem. Rev.*, 2001, **101**, 1963–1980.
49 E. S. Shubina, N. V. Belkova, A. N. Krylov, E. V. Voronstov, L. M. Epstein, D. G. Gusev, M. Niedermann and H. Berke, *J. Am. Chem. Soc.*, 1996, **118**, 1105–1112.
50 N. V. Belkova, P. O. Revin, L. M. Epstein, E. V. Vorontsov, V. I. Bakhmutov, E. S. Shubina, E. Collange and R. Poli, *J. Am. Chem. Soc.*, 2003, **125**, 11106–11115.
51 N. V. Belkova, E. Collange, P. Dub, L. M. Epstein, D. A. Lemenovskii, A. Lledós, O. Maresca, F. Maseras, R. Poli, P. O. Revin, E. S. Shubina and E. V. Vorontsov, *Chem.–Eur. J.*, 2005, **11**, 873–888.
52 M. Baya, O. Maresca, R. Poli, Y. Coppel, F. Maseras, A. Lledos, N. V. Belkova, P. A. Dub, L. M. Epstein and E. S. Shubina, *Inorg. Chem.*, 2006, **45**, 10248–10262.
53 H. S. Chu, C. P. Lau, K. Y. Wong and W. T. Wong, *Organometallics*, 1998, **17**, 2768–2777.
54 T. Liu, X. Wang, C. Hoffmann, D. L. DuBois and R. M. Bullock, *Angew. Chem., Int. Ed.*, 2014, **53**, 5300–5304.
55 B. C. Manor and T. B. Rauchfuss, *J. Am. Chem. Soc.*, 2013, **135**, 11895–11900.
56 L. M. Epstein, E. S. Shubina, A. N. Krylov, A. Z. Kreindlin and M. I. Rybinskaya, *J. Organomet. Chem.*, 1993, **447**, 277–280.
57 E. Peris and R. H. Crabtree, *J. Chem. Soc., Chem. Commun.*, 1995, 2179–2180.
58 N. V. Belkova, E. I. Gutsul, O. A. Filippov, V. A. Levina, D. A. Valyaev, L. M. Epstein, A. Lledos and E. S. Shubina, *J. Am. Chem. Soc.*, 2006, **128**, 3486–3487.
59 M. Schlaf, A. J. Lough, P. A. Maltby and R. H. Morris, *Organometallics*, 1996, **15**, 2270–2278.
60 T. P. Fong, C. E. Forde, A. J. Lough, R. H. Morris, P. Rigo, E. Rocchini and T. Stephan, *J. Chem. Soc., Dalton Trans.*, 1999, 4475–4486.
61 K. Gotoh, R. Ishikawa and H. Ishida, *Acta Crystallogr., Sect. E: Struct. Rep. Online*, 2005, **61**, o4016–o4017.
62 G. R. Juan Carlos, G. P. Carlos, N. Heinrich and F. P. Angelina, *Eur. J. Inorg. Chem.*, 2004, **2004**, 601–611.
63 C. Federsel, A. Boddien, R. Jackstell, R. Jennerjahn, P. J. Dyson, R. Scopelliti, G. Laurenczy and M. Beller, *Angew. Chem., Int. Ed.*, 2010, **49**, 9777–9780.
64 M. R. Ringenberg, F. Wittkamp, U.-P. Apfel and W. Kaim, *Inorg. Chem.*, 2017, **56**, 7501–7511.
65 M. Baya, P. A. Dub, J. Houghton, J.-C. Daran, N. V. Belkova, E. S. Shubina, L. M. Epstein, A. Lledós and R. Poli, *Inorg. Chem.*, 2009, **48**, 209–220.
66 A. E. Reed, L. A. Curtiss and F. Weinhold, *Chem. Rev.*, 1988, **88**, 899–926.

67 L. A. Curtiss, C. A. Melendres, A. E. Reed and F. Weinhold, *J. Comput. Chem.*, 1986, **7**, 294–305.
68 T. Liu, Q. Liao, M. O'Hagan, E. B. Hulley, D. L. DuBois and R. M. Bullock, *Organometallics*, 2015, **34**, 2747–2764.
69 M. J. Therien and W. C. Trogler, *J. Am. Chem. Soc.*, 1986, **108**, 3697–3702.
70 M. T. Olsen, T. B. Rauchfuss and S. R. Wilson, *J. Am. Chem. Soc.*, 2010, **132**, 17733–17740.
71 Y. Lee, R. A. Kinney, B. M. Hoffman and J. C. Peters, *J. Am. Chem. Soc.*, 2011, **133**, 16366–16369.
72 J. M. Camara and T. B. Rauchfuss, *J. Am. Chem. Soc.*, 2011, **133**, 8098–8101.